Modeling the shortening history of a fault-tip fold using structural and geomorphic records of deformation

Mathieu DAËRON — daeron@gps.caltech.edu
Division of Geological and Planetary Sciences, California Institute of Technology, USA
Jean-Philippe AVOUAC — avouac@gps.caltech.edu
Division of Geological and Planetary Sciences, California Institute of Technology, USA
Julien CHARREAU — julien.charreau@univ-orleans.fr
Institut des Sciences de la Terre d'Orléans, France
Stéphane DOMINGUEZ — dominguez@dstu.univ-montp2.fr
Laboratoire de Dynamique de la Lithosphère, ISTEEM, Montpellier, France
(Submitted to JGR on April 21, 2006)

Abstract

We present a methodology to derive the growth history of a fault-tip fold above a basal detachment. Our approach is based on modeling of the stratigraphic and geomorphic records of deformation, as well as the finite structure of the fold constrained from seismic profiles. We parametrize the spatial deformation pattern using a simple formulation of the displacement field derived from sandbox experiments. Assuming a stationary spatial pattern of deformation, we simulate the gradual warping and uplift of stratigraphic and geomorphic markers, which provides bounds on the cumulative amount of shortening they have recorded. This approach allows modeling of isolated terraces or growth strata. We apply this method to the study of two fault-tip folds in the Tien Shan, the Yakeng and Anjihai anticlines, documenting their deformation history over the past 6-7Myr. We show that the modern shortening rates can be estimated from the width of the fold topography provided that the sedimentation rate is known, yielding respective rates of 2.15mm/yr and 1.12mm/yr across Yakeng and Anjihai, consistent with the deformation recorded by fluvial and alluvial terraces. This study demonstrates that the shortening rates of both folds accelerated significantly since the onset of folding. It also illustrates the usefulness of a simple geometric folding model, and highlights the importance of considering local interactions between tectonic deformation, sedimentation and erosion.

1 Introduction

In regions of active folding and thrusting, cumulative deformation of geomorphic surfaces such as alluvial or fluvial terraces (figure 1) can be used to constrain modern rates of horizontal shortening [*Rockwell et al.*, 1988; *Lavé and Avouac*, 2000; *Thompson et al.*, 2002]. At deeper levels, pretectonic geologic units record finite shortening across the fold, while intermediate growth strata, deposited as the fold was already growing and sometimes exposed at the surface (figure 1), document the long-term shortening history [*Suppe et al.*, 1992; *Epard and Groshong*, 1993; *Hardy and Poblet*, 1994; *Storti and Poblet*, 1997; *Gonzalez-Mieres and Suppe*, 2006]. It should therefore be possible to retrieve the complete history of fold growth from the joined interpretation of the geomorphic record of recent deformation and the sub-surface structure of a fold.

Linking surface uplift to horizontal shortening can be challenging, however. Where a marker is preserved continuously across a fold, conservation of cross-sectional area allows estimating the cumulative horizontal shortening experienced by the marker, provided that the deep geometry of the underlying fault is known [*Lavé and Avouac*, 2000]. In many cases, however, geomorphic markers are not continuously observable, either due to erosion or to partial burying under younger sediments (figure 1). In that case, the "area conservation" method is not applicable. An alternative approach then consists in relying on some explicit function relating uplift to horizontal shortening. For example, in fault-bend folds, where bedding-parallel motion is expected, horizontal shortening can be equated to uplift divided by the sine of structural dip [*Lavé and Avouac*, 2000].

Such a formulation, however, is not always available for other types of fold, in particular for fault-tip folds, where rocks are deformed in a broad zone above the termination (or "tip") of a thrust fault [*Dahlstrom*, 1990; *Suppe and Medwedeff*, 1990; *Mitra*, 2003]. The sketch in figure 1 shows such an example, where horizontal shortening above the tip of a basal detachment is compensated by layer thickening, which manifests as warping and uplift of the surface. This pattern of deformation is observed in relatively young folds, because strain tends to localize after a certain amount of distributed shortening, and the system evolves towards a fault-bend fold [*Suppe*, 1983; *Avouac et al.*, 1993]. Although the situation depicted in figure 1 is similar to trishear fault-propagation folding [*Almendinger*, 1998], where deformation at the front of a fault-tip is modeled by distributed shear in a triangle, the trishear formulation does not apply directly in the case of a propagating detachment since it requires that the triangle contains the extrapolated fault plane, which is not the case in figure 1. Analog experiments by *Bernard et al.* [2006] support a simple analytical formulation of the displacement field produced by incremental shortening of such a system (appendix A), and this formulation has been used to analyze the growth of Pakuashan anticline along the western foothills of Taiwan [*Simoes et al.*, 2006]. In order to further explore this methodology, we use the same formulation to model the growth of two case examples of young fault-tip folds located in the fold-and-thrust belts that bound the Tien Shan range, in Central Asia, for which good seismic data are available [*Dengfa et al.*, 2005; *Hubert-Ferrari et al.*, 2005, 2006; *Gonzalez-Mieres and Suppe*, 2006]. The displacement model's parameters, which govern the finite shape of the fold, are estimated based on seismic imaging of deep pre-growth strata. The same seismic data is also used to constrain the finite amount of shortening and the stratigraphic depth of fold initiation. Assuming that the deformation pattern has not varied significantly over the fold's history, we use the parametrized displacement model to deform incrementally a cross-section of the fold, progressively adding syntectonic markers, so as to reproduce surface data such as present-day relief, the shape of alluvial and fluvial terraces, and field-measured structural dip angles. Comparing the predicted and observed finite geometries allows to test the validity of our assumptions regarding the initial geometry of markers, and to estimate the amount of shortening recorded by each of them. We emphasize that the objective of the present study is not to characterize in detail the history of two specific folds, but rather to lay out the requirements and potential benefits of our modeling approach.

2 Regional setting

The Tien Shan range, in Central Asia, is one of the highest and most rapidly deforming intracontinental mountain belts on Earth (figure 2). It stretches along 2500 km between the Tarim and Junggar basins, with peaks generally higher than 4500 m above sea level. Following a complex, subduction-related Paleozoic history [*Burtman*, 1975; *Windley et al.*, 1990], it was reactivated in the early Miocene [*Métivier and Gaudemer*, 1997; *Sobel and Dumitru*, 1997; *Bullen et al.*, 2001] as a long-term and long-range consequence of the indentation of India into Asia, and accommodated up to 200 km of cumulative Cenozoic shortening [*Avouac et al.*, 1993].

High levels of seismicity, GPS measurements and spectacular evidence of surface faulting and folding all attest to ongoing, rapid deformation. At the longitude of our study (83–86°E), the 6 mm/yr GPS shortening rate across the Tien Shan [*Reigber et al.*, 2001] is taken up by active faulting within the range and by two fold-and-thrust belts that mark its northern and southern boundaries (figure 2). In these piedmonts, over-thrusting of the Tarim and Junggar basins manifests as E-W alignments of active anticlines which deform alluvial and fluvial terraces. The frontmost folds (basin-wards) are the youngest. They generally form above blind detachments in the Mesozoic to Quaternary sediments of the foreland, and take up a significant part of the active shortening [*Avouac et al.*, 1993; *Molnar et al.*, 1994; *Burchfiel et al.*, 1999].

We selected two of these frontmost piedmont folds as modeling targets, seeking to take full advantage of the rapid deformation rates and of the wealth of available data (seismic reflection profiles, structural exposure by river incision, well-preserved alluvial and fluvial terraces, magnetostratigraphic time constraints). The first of these folds is the Yakeng anticline, a well-imaged fault-tip fold above a blind basal detachment, which has been the focus of previous investigations [*Poisson*, 2002; *Hubert-Ferrari et al.*, 2005, 2006; *Gonzalez-Mieres and Suppe*, 2006]. Our intent here is to make use of the tight existing structural constraints to model the geomorphic record of deformation. The Anjihai anticline is another example of a similar fold. Its geomorphic expression is comparable but not identical to that of Yakeng. Although the structure at depth of Anjihai is less tightly constrained, it constitutes a good target for our modeling approach because reliable seismic or geomorphic markers cannot be traced continuously across the fold, although there is abundant local evidence for growth strata and folded alluvial surfaces.

Our geometric modeling does not directly provide timing information. It does, however, yield stratigraphic constraints on the initiation and accumulation of shortening, which can then be converted to ages using the recent magnetostratigraphic studies of *Charreau et al.* [2005, 2006] and *Charreau* [2005]. These studies show evidence for remarkably constant sedimentation rates at the scale of several millions of years. In the Yaha section (southern piedmont), less than 20 km upstream from the Yakeng fold, they measured an average sedimentation rate of 0.43 mm/yr over the period from 10 to 5 Ma [*Charreau et al.*, 2006]. In the Kuitun He section (northern piedmont), they found evidence for a constant rate of 0.21 mm/yr from 10 to 3 Ma [*Charreau et al.*, 2005], and for a 10–9 Ma rate of 0.27 mm/yr in the Jingou He section [*Charreau*, 2005], 40 km east of the previous and less than 20 km upstream from Anjihai. Overall, these results imply that "old" rates (younger than 10 Ma) may be extrapolated over millions of years, up to at least 3 Ma, yielding estimated recent sedimentation rates of 0.43 mm/yr near Yakeng and 0.27 mm/yr near Anjihai.

3 Yakeng

3.1 Description

The Yakeng anticline stretches for ∼100 km east of the town of Kuqa, along the southern Tien Shan piedmont (figures 2 and 3). At the surface, it manifests as a gentle, 5-to-10-km-wide, ∼150-m-high ridge resulting from the folding of a large-scale, south-dipping alluvial terrace, noted Ta, whose age is loosely constrained to be older than ∼34 ka from OSL dating [*Poisson*, 2002]. Ta is generally well preserved, although south-flowing rivers dissect it in a number of locations, forming steep, narrow gorges. The Yakeng cross-section discussed below corresponds to the ridge-perpendicular seismic profile reported on the map in figure 3, and shown in figure 4. About 10 km to the east of the profile, Ta is incised by the East Quilitag river, which formed and abandoned a partially preserved fluvial terrace (Tf). Since then, ongoing deformation has folded and uplifted Tf, bringing it about 25 m above the modern river [*Poisson*, 2002]. Although the age of Tf is unknown, *Poisson* [2002] inferred it to be similar to that of another fluvial terrace near Kuqa, OSL-dated to 10.6$\pm$1 ka.

Seismic imaging (figure 4) reveals that the width of the subsurface fold is more than twice that of the emergent Ta, because the latter is buried under sediments on the outer flanks of the anticline. At depth the amplitude of folding generally decreases downwards, consistent with the geometry of a fault-tip detachment fold growing above a 6-km-deep basal detachment coinciding with reflector L4, in the evaporites of the Oligo-Miocene Jidikeh formation [*Hubert-Ferrari et al.*, 2005]. Because of a complex basement geometry below the anticline, and due to the proximity of the Yanan fold, it is not straightforward to use traditional area relief methods to analyze shortening across Yakeng. However, *Gonzalez-Mieres and Suppe* [2006], using measurements of thickness relief area, estimated 1.2 km of finite shortening, and showed that folded reflectors L5 to L14 are pretectonic.

3.2 Parameters of the deformation model

While the geometric complexity of the deep part of the fold justifies studying it in the thickness domain [*Gonzalez-Mieres and Suppe,* 2006], our incremental deformation approach requires explicit definition of the initial undeformed geometry of each marker. Considering that the analysis of *Gonzalez-Mieres and Suppe* [2006] is reliable, we assume a priori that L14 is the youngest pretectonic reflector, while L15 and above are syntectonic. In order to parametrize our displacement field model, we only consider the syntectonic units, because the irregular shape of pretectonic markers obscure the pattern of deformation below L15.

To define the initial, undeformed geometry of seismic reflectors L15 to L27, we consider two zones which we assume to be unaffected by the Yakeng anticline (gray boxes in figure 5). The slopes of markers upstream from the fold are systematically steeper than downstream of it ($\sim$3% versus 1%), which precludes approximating the initial geometries as straight lines. Fitting independently each reflector using a higher-order polynomial would yield geometries with different curvatures from one reflector to another, generating unrealistic thickness changes and obscuring the variation of relief area as a function of depth. To address these issues, we call upon a two-stage approach. First we fit each undeformed marker, independently from one other, using a straight line. The 13 independent linear fits, noted LF15 to LF27, have different slopes, all consistent with basin-ward thinning of alluvial deposits. The 13 sets of depth residuals (dZ) are then aggregated into one set of (X,dZ) values, which reflects invariant slope increase across the fold, and the aggregated set is fit using a single second-order polynomial, noted PF. The initial geometry of each reflector Li is approximated as the sum of the corresponding linear fit LFi and the common parabolic fit PF. This ensures that individual thickness variations and upstream steepening are consistent with those observed, while avoiding unrealistic thickness disparities from one layer to the other in the core zone. The resulting set of fits, noted U15 to U27, is then used in our model to represent the initial geometries of the syntectonic reflectors.

We then quantify the cumulative shortening of reflectors L15 to L27 using the excess area method of *Epard and Groshong* [1993]. Figure 6 shows the resulting amounts of shortening. Assuming a 0.43 mm/yr sedimentation rate [*Charreau et al.*, 2006], a linear fit of shortening versus depth is consistent with an average shortening rate of $\sim$0.14 mm/yr over a period extending from $\sim$5.8 to 2.1 Ma. The observed scatter is likely due to the approximation of our simplified initial geometry, and possibly to the uncertainties of the seismic reflection data. The regression plotted in figure 6 is then used to define the amounts of shortening ascribed to each syntectonic reflector, with an uncertainty of $\pm$70 m (dashed lines). For comparison, using the same sedimentation rate, the analysis by *Hubert-Ferrari et al.* [2006] of thickness variations in the same syntectonic layers yields a similar shortening rate of 0.12–0.13 mm/yr.

Based on the initial geometry of seismic markers and their respective amounts of shortening, it is now possible to choose parameters of the displacement field model (hinge line positions and [alpha] values, see appendix A) which predict deformed geometries consistent with that observed in the seismic profile. The fold's subsurface width does not decrease significantly with depth, suggesting that the folding pattern is self-similar in cross-section, as discussed by *Hubert-Ferrari et al.* [2006]. For this reason, we use only vertical hinge lines to parametrize the displacement model. While it is possible to obtain a approximate fit of the geometries of L15–27 using a 7-hinge model, the resulting parameters are heavily influenced by the bulge in the shapes of L15–19 south of the fold, which probably reflects an inherited geometry. Moreover, the L27 geometry predicted by this model is somewhat approximate. Since L27 is remarkably similar in shape to the topography of Ta, we opted to use a set of parameters which closely fit L27 at the expense of a lower-quality fit to the deepest syntectonic markers (figure 7). This model was then used to estimate the initial geometries and cumulative shortening of the geomorphic markers.

3.3 Original geometry and cumulative shortening of geomorphic markers

Our model allows predicting the acquired slope after an arbitrary amount of deformation, so we can use this prediction to estimate the shortening and local uplift experienced by each of these surfaces. We have no precise a priori information on the initial elevation of Ta and Tf. We can, however, place realistic constraints on their initial slopes.

The initial, undeformed geometry of the partially preserved fluvial terrace Tf must reflect that of the paleo-river. We infer that its original slope lies somewhere between the local slope of the modern East Quilitag river below Tf (1.3%) and the average slope along the whole length of the gorge across the fold (1.6%). Considering an initial marker with such a dip angle, we systematically vary its initial elevation and the amount of shortening it recorded, using the deformation model determined above, and compare the predicted elevation and dip to those of Tf. For an initial slope of 1.3%, between 55 and 65 m of shortening are necessary to tilt and uplift the initial marker so that the deformed geometry fits the observed geometry of Tf (figure 8). This corresponds to an initial elevation 20–26 m below the modern-day river, and to $\sim$40 m of local uplift. For a steeper initial dip of 1.6%, the modeled amount of shortening is 75–85 m, with an initial level 33–40 m below the modern-day river, corresponding to over 50 m of local uplift. Note that the modeled local uplifts are significantly larger than the apparent uplift of $\sim$17 m, because the modern-day river runs at a higher elevation than that when Tf was formed, presumably because of ongoing sedimentation downstream and upstream of the fold.

Estimating the original slope of the alluvial terrace Ta is somewhat less straightforward. It could be argued that, as an alluvial terrace similar to the youngest seismic markers (L27 and below), its initial profile should resemble that of U27, the initial profile of L27. However, modeling the incremental folding of such a marker (parallel to U27 but with appropriate initial elevation), results in a predicted profile higher than the actual topography on the north flank of the fold, and lower on the south flank (figure 9). This is clear indication that the assumed initial geometry dips too steeply to the south. An alternative assumption is that Ta corresponds to a paleo-surface of a fan fed by the east Quilitag river, with a slope similar to that of the modern dark grey fan upstream of the anticline (figure 3). This would allow for a predicted geometry more similar to the observed topography, but the synthetic profile still lies above the northern flank and below the southern flank of the fold. While this could result solely from a faulty assumption that the deformation is vertically self-similar, it more probably reflects that Ta was aggraded at the surface of a paleo-fan predating the emergence of the topographic expression of the fold, with a slope on the order of 1.3%, less steep than the modern upstream fan. Such an initial dip allows for a good fit of the modern Ta geometry using our deformation model, consistent with about 300 m of cumulative shortening. Despite the uncertainty on the original slope of Ta, the amount of shortening required to tilt the north flank of the fold up to its current dip (5% to the north) appears to be rather robust, on the order of 300–330 m.

3.4 Growth of the Yakeng fold, and its influence on drainage and sedimentation

Our modeling of the Yakeng anticline highlights the importance of accurately estimating the initial geometry of folded geomorphic markers. Assuming that ongoing deformation is similar to the finite folding, the present-day shape of the Yakeng ridge appears to put tight constraints on the original slope of Ta (figure 9). Rather than an artifact of our particular model, this is a general consequence of the self-similarity of deformed markers noted by *Hubert-Ferrari et al.* [2006]. Further work is now needed to test this prediction by direct observation, possibly through shallow seismic imaging.

Whatever the precise original geometry of Ta, it seems unavoidable that its initial slope was much shallower than that of L27, the youngest continuous seismic reflector. A tentative explanation to the discrepancy might be that seismic reflectors beneath Yakeng experienced some tilting as a result of the growth of the Quilitag anticline [*Hubert-Ferrari et al.*, 2006]. If this is the case, whether tilting occurred prior to or during the development of Yakeng does not affect our analysis, provided that the assumed initial geometries correctly reflect the effect of Quilitag folding.

The current geometry of Tf and Ta imply that since their emplacement they recorded cumulative shortening on the order of 70 and 300 m, respectively. In theory, provided some knowledge of the sedimentation rate, one could deduce their ages from their reconstructed initial geometries. However, if indeed the slope of Ta is similar to that predicted in figure 9C, the thickness of post-Ta sediments upstream of the fold is about twice as thick as downstream of it, which could be readily interpreted as resulting from emergence of relief, the ridge acting as a dam. Such a hydrographic disruption would likely perturb the constant sedimentation regime documented by *Charreau et al.* [2006]. The Yaha sedimentation rate is thus not a reliable indicator of the ages of alluvial surfaces which were formed after topographic emergence of the Yakeng ridge, including Ta. Age constraints on Ta and Tf should thus be obtained through direct dating methods (OSL, cosmogenic isotopes), and their reconstructed depths can only provide very loose age constraints. Accordingly, if we assume that the sedimentation rate was mostly perturbed upstream of the fold, the reconstructed position of Ta downstream of the fold ($\sim$75 m below the surface) suggests an age on the order of 175 kyr. This estimate would correspond to an average post-Ta shortening rate of about 1.7 mm/yr, more than ten times faster than the longer term rate (0.14 mm/yr, see figure 6). Conversely, if a current shortening at a rate comparable to the long-term average is assumed, it implies ages for Tf and Ta of respectively 500 kyr and more than 2 Myr, inconsistent with the available geomorphic and lithological evidence. The shortening across Yakeng has thus necessarily accelerated significantly in geologically recent times, although better quantifying the modern rate will require direct dating of Tf and Ta.

4 Anjihai

4.1 Surface expression and finite shortening

The Anjihai anticline lies frontmost in the fold-and-thrust belt along the northern Tien Shan piedmont (figures 2 and 10). The surface fold is about 7 km wide, and exposes conglomerates of the Xiyu (Lower Pleistocene) and Dushanzi (Pliocene) formations, unconformably overlain by Quaternary conglomerates and loess (figure 11). On the flanks of the anticline, such Quaternary structural surfaces are well-preserved, forming triangular cuestas with slopes of 7–10%. We interpret these surfaces (noted Tn and Ts) as folded abrasion terraces (green line segments in figures 11 and 12), dating back to a time when the erosion power of the Anjihai He and/or Jingou He rivers was strong enough to remove emergent relief as the fold was growing. The abrasion terraces were later abandoned and started passively recording deformation. This was likely coeval with entrenchment of a river channel across the fold, originally by the Jingou He and today by the Anjihai He. Along the steep walls of the river-gap, the shallow structure of the fold is beautifully exposed, with dip angles up to 25^{o} (figure 11).

The seismic profile run along the Anjihai river (figure 12) reveals a smooth, rather symmetric subsurface structure strongly suggestive of detachment-driven folding. The seismic data was only made available in double-time domain, and we performed a first-order conversion to depths using an uniform seismic velocity of 2.5 km/s. While this is probably an unrealistic approximation, different competing assumptions on the velocity structure of the fold (lithology- versus compaction-driven velocities) would yield different depth-converted sections and affect our analysis. For now, we use this crude depth correction, not so much as a reliable indication of the fold's deeper geometry, but as a starting point to demonstrate the potential of our approach.

Our line-drawing interpretation of the seismic data (figure 12) allows mapping 7 distinct markers across the fold (L1 to L7). These markers are linear away from the fold, making it straightforward to infer their original, undeformed geometry. For all seven markers, the structural relief areas are well-correlated with depth, consistent with 1.553 km of finite shortening over a basal detachment located

$\sim$5 km below the surface (4.5 km b.s.l., see figure 13). We conclude that the sediments below L7 are pretectonic strata, which yields a lower stratigraphic bound for the initiation of folding, 2.0 km below the surface. This depth corresponds to an age of 7.4 Ma, according to the 0.27 mm/yr sedimentation rate derived form the magnetostratigraphies of *Charreau et al.* [2005] and *Charreau* [2005].

4.2 Parameters of the deformation model

Imposing a finite shortening of 1.55 km and a basal detachment depth of 4.5 km b.s.l., we can model the observed finite geometry of the pretectonic markers using the fold kinematics discussed in appendix A. A good fit of the seismic data is obtained with 12 inter-hinge domains. A graphical illustration of the agreement between the predicted and observed dip angles is shown in figure 15, where all present-day seismic reflectors were retro-deformed according to our best-fitting model parameters. Below L7, the retro-deformed reflectors are uniformly flat, whereas above L7 they adopt a syncline-like geometry, implying that the actual amount of shortening experienced by these these markers is smaller than the finite amount. These reflectors must therefore correspond to growth strata.

4.3 Early shortening history and evidence for Quaternary acceleration

In order to account for the progressive emplacement and shortening of the seismic reflectors above L7, we tested simple scenarios of shortening, by postulating a constant shortening rate, a constant sedimentation rate, and by varying the stratigraphic level of fold initiation. We could obtain a good fit to the seismic data from this approach. However, all of these models predict that the fold should have no or negligible topographic relief, because the sedimentation rate, well-constrained to $\sim$0.27 mm/yr by *Charreau* [2005], generally exceeds the uplift rate (figure 16). As an additional consequence, it is impossible to reproduce the structural dip angles observed along the cliff incised by the Anjihai He river, because the model does not allow for a cliff to form. This is clear indication that the ratio of shortening to sedimentation rates has recently increased. Nevertheless, the geometry of seismic reflectors above L7 supports early initiation of folding, albeit with average rates no faster than 0.4 mm/yr between the deposition of L7 and that of the shallowest seismic reflectors (from 1.25 km b.s.l. to 0.5 km a.s.l., i.e. roughly from 7.4 to 0.9 Ma).

The shallowest seismic reflectors are too deep to have unambiguously recorded any recent acceleration of shortening. In the absence of well-preserved fluvial terraces across the fold, the only available geomorphic markers are the abrasion terraces Tn and Ts. It is probable that, although the core of the fold has been eroded, they were probably originally connected, forming one continuous terrace tread Ta. Unfortunately, the undeformed depth and slope of Ta are unconstrained. Using the same kinematic deformation model as above, and assuming the original slope of Ta was similar to that of the modern topography, roughly 500 m of shortening are necessary to fit the present geometry of Ts (figure 17). However, in this scenario the predicted position of Ta does not coincide with Tn. Indeed, it is striking that, contrary to the Yakeng fold, the finite anticline and the topographic relief are not co-located. While this could be interpreted as evidence that the deformation pattern has changed during the fold growth, this is not a unique explanation. The 1-km offset between the axis of the structural anticline and the center of the Anjihai ridge might in fact reflect that the original slope of Ta was steeper than we inferred. Alternatively, the discrepancy might result from Tn and Ts having different ages of abandonment.

4.4 Growth history of the Anjihai fold

Although some aspects of the study should be re-assessed once better depth constraints on the seismic data and better chronological constraints become available, the first-order results of our model are not expected to depend qualitatively on a specific seismic velocity conversion. Building up the observed topography does requires a recent acceleration of uplift, because the early rate of deformation recorded by syntectonic seismic reflectors is too slow to generate significant relief (figure 16). Furthermore, the acceleration must predate the emplacement of Tn, as evidenced by the abrasion of underlying units (figure 11).

It also appears that modeling terraces Tn and Ts as a single surface emplaced parallel to the modern alluvial topography is inconsistent with their observed present-day geometry. Again, this could reflect a different initial slope than assumed, which could also explain why the axis of the anticline observed in surface structural dips differs from the axis of symmetry of Tn and Ts (figure 11). In this case, however, the predicted original slope would need to be steeper than the modern topography surrounding the fold, which might result from the complex capture history of the Anjihai He river [*Poisson*, 2002].

5 Discussion

5.1 Competition between folding and sedimentation

The study of these case examples highlights some simple interactions between folding, sedimentation and erosion, summarized in figure 18. Topographic relief can only accrue where and when tectonic uplift is faster than sedimentation (see also discussion in *Simoes et al.* [2006]). Thus, in the early phases of the histories of both folds, syntectonic sedimentary units extend continuously across the fold, and no topographic relief builds up (figure 18A). As shortening rate increases, maximum uplift rates overcome the sedimentation rate, in a zone whose width is a function of the spatial distribution of uplift. As long as the hydrographic system has enough erosion power to sweep laterally back and forth and abrade rocks as they are uplifted, relief remains negligible, and an abrasion surface is emplaced, unconformably overlying older units (figure 18B), as observed on the northern flank of Anjihai (figure 11A). If the river is forced to entrench in a narrow gorge because it does not have enough stream power excess to abrade laterally all the uplifted rocks, relief starts building up above the core of the anticline (figure 18C). Figure 19 shows a sketch summarizing the appearance of the fold at that stage, which corresponds to the current situation of Yakeng. Eventually, the fold ridge is expected to undergo secondary erosion driven by its own relief, as observed in the exposed core of Anjihai.

5.2 Estimating shortening rate from fold width

One quantitative consequence of this qualitative scenario is that topographic relief width is a simple function of the spatial distribution of uplift and the sedimentation rates. Shortly after initiation of relief emergence, the fold width should equate to the width of the area where the uplift rate is greater than the sedimentation rate. Using our models of deformation for the Yakeng and Anjihai folds, we plot in figure 20 the predicted fold width as a function of this ratio. The ratios consistent with the observed fold widths are 5.0 for Yakeng, and 4.15 for Anjihai. Combining this information with the relevant magnetostratigraphic sedimentation rates yields first-order estimates of the mean shortening rates since relief emergence, 2.15 mm/yr at Yakeng and 1.12 mm/yr at Anjihai, both much faster than the long-term averages (respectively estimated to $\sim$0.17 and 0.2–0.4 mm/yr). Furthermore, at Yakeng, if the cumulative shortening experienced by Ta is indeed of the order of 300 m (figure 9C), its age can be estimated from the 2.15 mm/yr shortening rate, which would yield $\sim$140 kyr, comparable to the $\sim$175 kyr estimated using the sedimentation rate downstream of the fold. While the precision and reliability of this fold-width method depend on our ability to understand the complexities of the post-emergence sedimentation regime, surface fold width stands out as a remarkably sensitive measurement, governed as it is by competition between two important geomorphic processes.

5.3 Evidence for distributed strain and strain weakening during fault-tip folding

In both cases analyzed here, as well as in the study of Pakuashan anticline [*Simoes et al.*, 2006], we find that the stratigraphic and geomorphic record of fold growth are reasonably well modeled from our analytical formulation which assumes linearly distributed shortening across the fold zone. In addition, in all three cases, cumulative strain is about 10–12%, suggesting that the model applies at least up to that level strain. Furthermore, the two cases offer compelling evidence that the shortening rates must have increased during folding. We suspect that this behavior reflects strain weakening during in the early stage of folding, when the underlying thrust fault is still blind. The slow, early stage of folding might correspond to a period of maturation during which rocks are progressively softened by damage, before strain migrates basin-wards. This phase must result from a gradual transfer of strain to the frontal folds, from more mature fold-and-thrust structures (Quilitag and Huo'erguosi anticlines respectively). Better understanding of such behavior will likely require comparing the shortening histories of adjacent fold-and-thrust systems, using similar methods as that discussed here [see also *Hubert-Ferrari et al.*, 2006].

6 Conclusion

The two case examples detailed in this study illustrate the merits of analyzing the stratigraphic and geomorphic record of folding using a quantitative geometric description of folding. This approach makes it possible to estimate cumulative shortening recorded by markers that are only locally observed, whereas the excess area method only applies to isochronous markers which can be traced continuously across the fold. Moreover, the method itself does not rely on a specific analytical description of displacements, and could thus be used to test various descriptions of fold deformation. Most importantly, our approach provides a framework in which to combine shortening data from various sources — surface morphology, structural outcrops, seismic profiles —, which document folding over very different time scales, thus offering an opportunity to study long-term variations of tectonic rates.

APPENDIX

A Displacement field model

Analog modeling by *Bernard et al.* [2006], using sandbox experiments, supports a simple first-order description of the cross-sectional velocity field above a detachment fault-tip fold. Their formulation describes horizontal and vertical components of motion as varying linearly in space within a series of (X,Z) domains bounded by hinge lines. In the early stage of fold development (i.e. before the system evolves towards more localized strain), the observed locations of the hinge lines vary little, while material passes through them from one domain to the next, consistent with a stationary approximation of the velocity field.

Using this purely kinematic description of deformation, one can incrementally model the progressive folding arbitrary geometric objects. While the analytical expression of velocities constitutes a simplification of the natural fold system, it is generally possible to fit the finite geometries of real-world folds, using only a limited number of model parameters. For instance, *Simoes et al.* [2006] used this approach to reconcile the finite and incremental deformation recorded by the Pakuashan anticline, in western Taiwan, and to estimate the finite amount and modern rate of shortening across the fold.

The model's reference frame is a 2D cross-section of the fold, similar to that shown in figure 1, where the footwall is fixed. In this plane, X is horizontal, increasing towards the footwall, and Z is vertical, increasing upwards. The X and Z components of velocity are noted Vx and Vz. Velocities far "ahead" (footwall-wards) of the fold or below the detachment level (Z<Zd) are nil. Velocities far "behind" the fold and above Zd are uniform and horizontal, equal to the slip rate on the detachment. Between these two blocks, in the folding area, Vx and Vz are continuous functions of (X,Z) which vary with X and Z in a series of spatial domains bounded by hinge lines (H1, H2, ...).

Along any arbitrary horizontal line (AA'), Vx varies linearly from Vs (the total rate of shortening across the fold) on the first hinge line, H1, to zero on the last hinge line Hn (figure A1). In the model, Vx is thus entirely defined by the total shortening rate and the positions of the first and last hinges. Along the same line (AA'), Vz varies linearly with X in each inter-hinge domain (figure A1), and dVz/dX is proportional to the height above detachment:

dVz/dX = [alpha].(Z-Zdetach)

The parameter [alpha] differs from one inter-hinge domain to another, but is constant within in each domain. As a result of the dip of hinge lines, Vz(Z) has a small quadratic component, but in the particular case where all hinge lines are vertical, Vz varies linearly with Z.

Acknowledgments

We are most grateful to John Suppe, Aurélia Hubert-Ferrari and Ramon Gonzalez-Mieres for sharing their results with us ahead of publication. We are also indebted to John Suppe and Martine Simoes for fruitful discussion This study was partly funded by the Gordon and Betty More Foundation. This is Caltech Tectonics Observatory contribution XXXX.

References

Almendinger, R. (1998), Inverse and forward numerical modeling of trishear fault propagation folds, *Tectonics*, *17*, 640–656.

Avouac, J.-P., P. Tapponnier, M. Bai, H. You, and G. Wang (1993), Active thrusting and folding along the Northern Tien-Shan and Late Cenozoic rotation of the Tarim relative to Dzungaria and Kazakhstan, *Journal of Geophysical Research*, *98*(B4), 6755–6804.

Bernard, S., J.-P. Avouac, S. Dominguez, and M. Simoes (2006), Kinematics of fault-related folding derived from a sandbox experiment, *Journal of Geophysical Research*, in prep.

Bullen, M., D. Burbank, J. Garver, and K. Abdrakhmatov (2001), Late Cenozoic tectonic evolution of the northwestern Tien Shan: new age estimates for the initiation of mountain building, *Geological Society ff America Bulletin*, *113*(12), 1544–1559.

Burchfiel, B., E. Brown, Q. Deng, X. Feng, J. Li, P. Molnar, J. Shi, Z. Wu, and H. You (1999), Crustal shortening on the margins of the Tien Shan, Xinjiang, China, *International Geology Review*, *41*(8), 665–700.

Burtman, V. (1975), Structural geology of Variscan Tien Shan, USSR, *American Journal of Science*, *A275*, 157–186.

Charreau, J. (2005), Evolution tectonique du Tianshan au Cénozoïque liée à la collision Inde-Asie : apport de la magnétostratigraphie et de la géochronologie isotopique U-Th/He, Ph.D. thesis, Université d'Orléans.

Charreau, J., Y. Chen, S. Gilder, S. Dominguez, J.-P. Avouac, S. Sen, D. Sun, Y. Li, and W. Wang (2005), Magnetostratigraphy and rock magnetism of the Neogene Kuitun He section (northwest China): implications for Late Cenozoic uplift of the Tianshan mountains, *Earth and Planetary Science Letters*, *230*, 177–192.

Charreau, J., S. Gilder, Y. Chen, S. Dominguez, J.-P. Avouac, S. Sen, M. Jolivet, Y. Li, and W. Wang (2006), Magnetostratigraphy of the Yaha section, Tarim Basin (China): 11Ma acceleration in erosion and uplift of the Tian Shan mountains, *Geology*, *34*(3), 181–184, doi:10.1130/G22106.1.

Dahlstrom, C. D. A. (1990), Geometric constraints derived from the law of conservation of volume and applied to evolutionary models for detachment folding, *American Association of Petroleum Geologists Bulletin*, *74*(3), 336–344.

Dengfa, H., J. Suppe, Y. Geng, G. Shuwei, H. Shaoying, S. Xin, W. Xiaobo, and Z. Chaojun (2005), Guidebook for field trip in South and North Tianshan foreland basin, ZinJiang Yugur Autonomous Region, China.

Epard, J., and R. Groshong (1993), Excess area and depth to detachment, *American Association of Petroleum Geologists Bulletin*, *77*(8), 1291–1302.

Gonzalez-Mieres, R., and J. Suppe (2006), Relief and shortening in detachment folds, *(submitted)*.

Hardy, S., and J. Poblet (1994), Geometric and numerical model of progressive limb rotation in detachment folds, *Geology*, *22*, 371–374.

Hubert-Ferrari, A., J. Suppe, X. Wang, and C. Jia (2005), The Yakeng detachment fold, South Tianshan, China, in *Seismic interpretation of contractional fault-related folds*, edited by J. Shaw, J. Connors, and J. Suppe, American Association of Petroleum Geologists.

Hubert-Ferrari, A., J. Suppe, R. Gonzalez-Mieres, and X. Wang (2006), Active folding of the landscape in the southern Tianshan, China, *(submitted)*.

Lavé, J., and J.-P. Avouac (2000), Active folding of fluvial terraces across the Siwaliks Hills, Himalayas of central Nepal, *Journal of Geophysical Research*, *105*(B3), 5735–5770.

Métivier, F., and Y. Gaudemer (1997), Mass transfer between eastern Tien Shan and adjacent basins (central Asia): constraints on regional tectonics and topography, *Geophysical Journal International*, *128*, 1–17.

Mitra, S. (2003), A unified kinematic model for the evolution of detachment folds, *Journal of Structural Geology*, *25*(10), 1659–1673.

Molnar, P., et al. (1994), Quaternary climate-change and the formation of river terraces across growing anticlines on the north flank of the Tien-Shan, China, *Journal of Geology*, *102*, 583–602.

Poisson, B. (2002), Impact du climat et de la tectonique sur l'évolution géomorphologique d'un piémont. exemple du piémont Nord du Tien Shan depuis la fin du Pléistocène, Ph.D. thesis, Université de Paris XI.

Reigber, C., et al. (2001), New space geodetic constraints on the distribution of deformation in central asia, *Earth and Planetary Science Letters*, *191*(1-2), 157–165.

Rockwell, T., E. Keller, and G. Dembroff (1988), Quaternary rate of folding of the Ventura Avenue anticline, western Transverse Ranges, southern California, *Geological Society of America Bulletin*, *100*(6), 850–858, doi:10.1130/0016-7606(1988)100<0850:QROFOT>2.3.CO;2.

Simoes, M., J.-P. Avouac, Y.-G. Chen, A. Singhvi, C.-Y. Chan, J. M., Y.-C. Chan, and S. Bernard (2006), Kinematic analysis of the Pakuashan fault-tip fold, West Central Taiwan: shortening rates and age of folding inception, *submitted*.

Sobel, E. R., and T. A. Dumitru (1997), Thrusting and exhumation around the margins of the western Tarim basin during the India-Asia collision, *Journal of Geophyical Research*, *102*(B3), 5043–5063.

Storti, F., and J. Poblet (1997), Growth stratal architectures associated to decollement folds and fault-propagation folds. inferences on fold kinematics, *Tectonophysics*, *282*(1–4), 353–373.

Suppe, J. (1983), Geometry and kinematics of fault-bend folding, *American Journal of Science*, *283*, 684–721.

Suppe, J., and D. A. Medwedeff (1990), Geometry and kinematics of fault-propagation folding., *Eclogae Geologicae Helvetiae*, *83*(3), 409–454.

Suppe, J., G. T. Chou, and S. C. Hook (1992), Rates of folding and faulting determined from growth strata, in *Thrust Tectonics*, edited by K. R. McClay, Chapman & Hall.

Thompson, S., R. Weldon, C. Rubin, K. Abdrakhmatov, P. Molnar, and G. Berger (2002), Late Quaternary slip rates across the central Tien Shan, Kyrgyzstan, central Asia, *Journal of Geophysical Research*, *107*(B9), 2203, doi:10.1029/2001JB000596.

Windley, B., M. Allen, C. Zhang, Z. Zhao, and G. Wang (1990), Paleozoic accretion and Cenozoic redeformation of the Chinese Tien Shan Range, central Asia, *Geology*, *18*(2), 128–131.

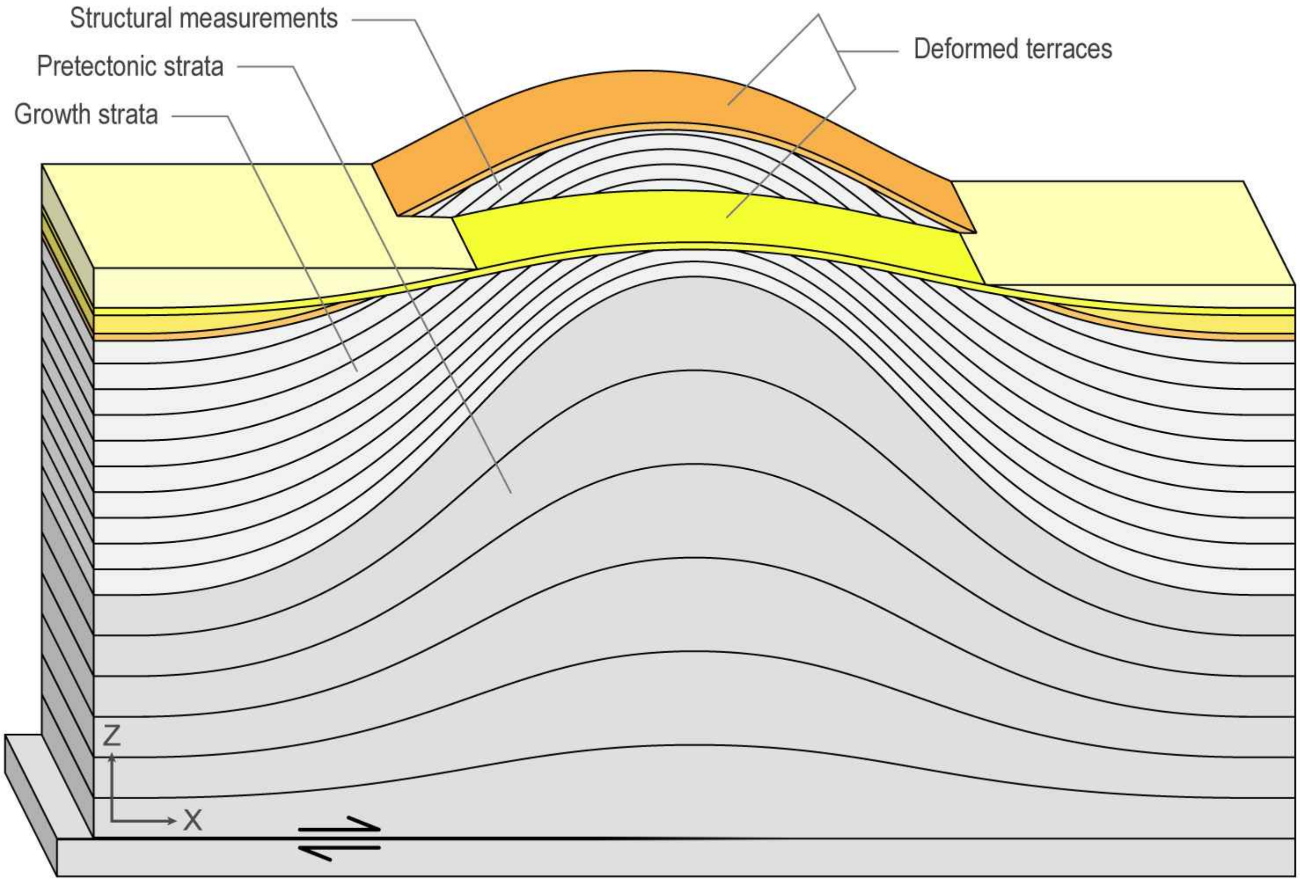

Figure 1: Synthetic sketch of the structural and geomorphic record of deformation, in the case of fold formed at the tip of a detachment fault.

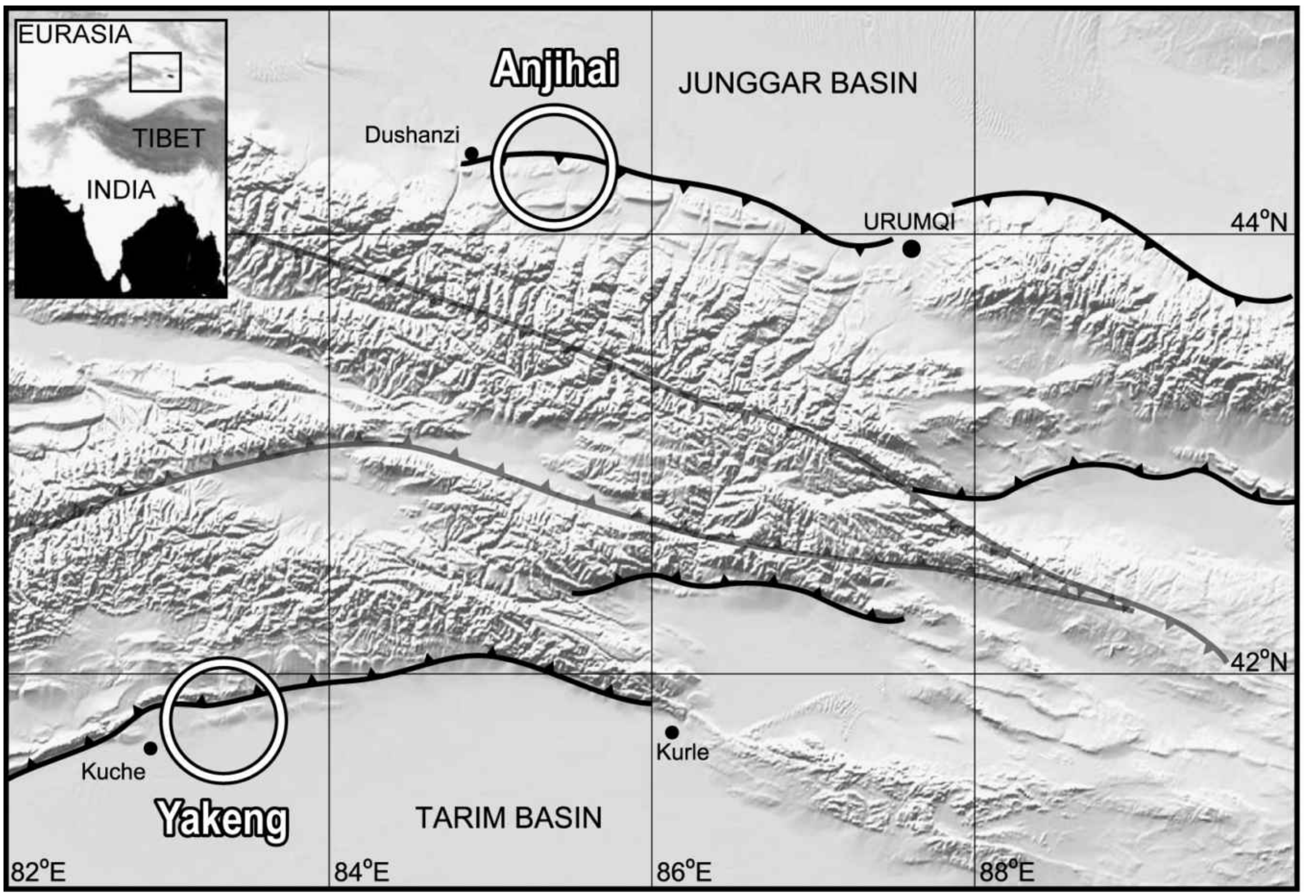

Figure 2: Map of the eastern Tien Shan area. White circles mark locations of the folds modeled in this study. Thick line show approximate location of zones of active thrusting and folding. Grey lines show location of the north Tien Shan and south Tien Shan suture zones (modified from *Charreau et al.* [2005].

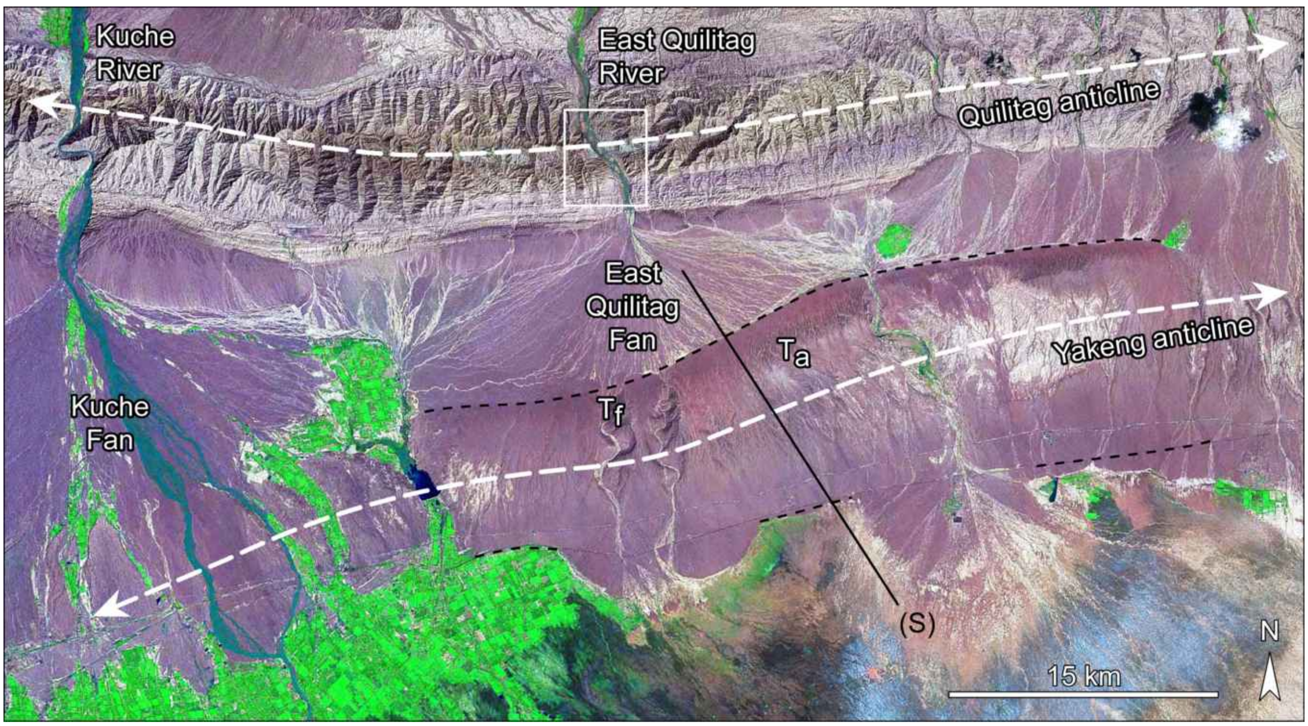

Figure 3: Map of Yakeng area. Solid black line (S) marks location of seismic profile [*Dengfa et al.*, 2005]. Dashed black line follows the outline of alluvial terrace Ta. “Tf” label shows location of preserved sections of fluvial terrace Tf (not mapped at this scale). White box shows the location of the magnetostratigraphic section of *Charreau et al.* [2006].

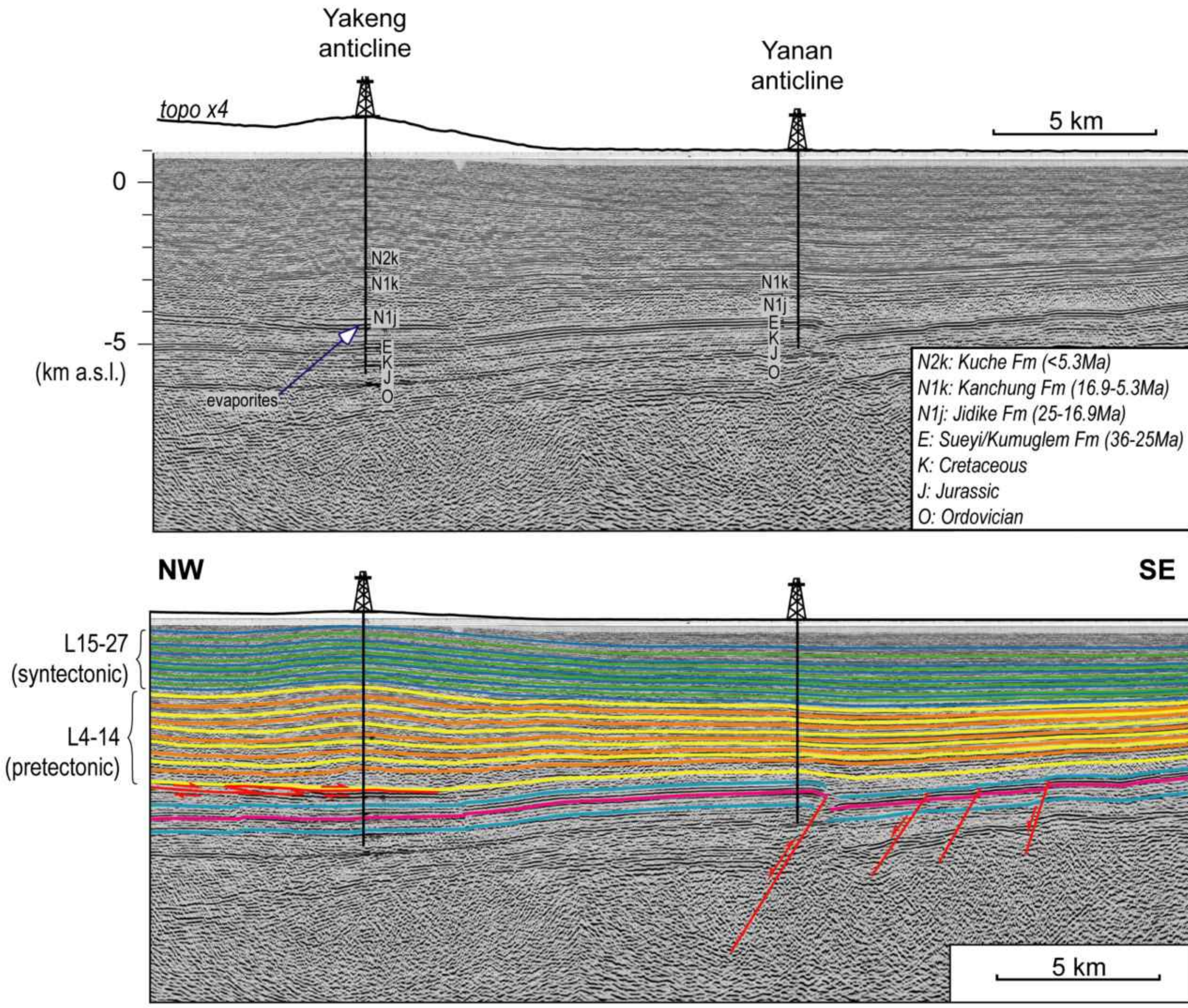

Figure 4: Seismic data and interpretation of Yakeng fold, from *Hubert-Ferrari et al.* [2005].

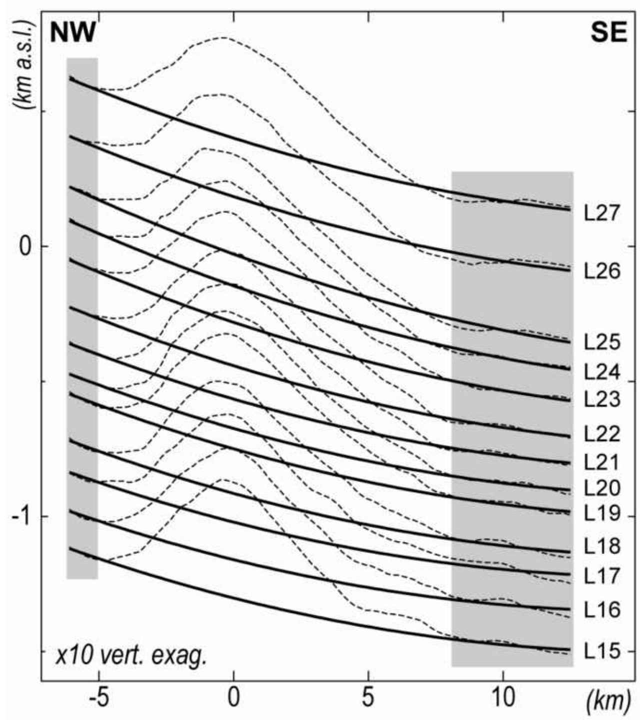

Figure 5: Regression of the original geometry of syntectonic seismic markers across Yakeng anticline. These second-order polynomial fits are constrained by data points away from the fold (gray boxes), and have different linear trends but a common quadratic component, thus similar curvatures (see details in text).

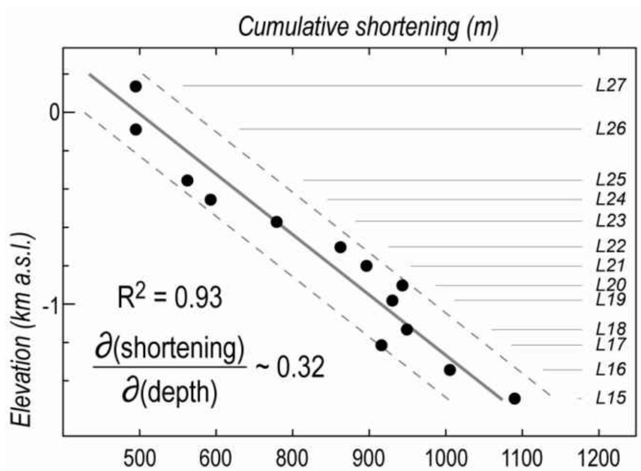

Figure 6: Yakeng shortening history recorded by syntectonic seismic markers. Cumulative shortening decreases linearly from 1.1 to 0.6 km between L15 (1.5 km b.s.l.) and L27 (0.1 km a.s.l.). Based on the 0.43 mm/yr sedimentation rate of *Charreau* [2005], this is consistent with an average shortening rate of 0.14 mm/yr over ~3.7 Ma.

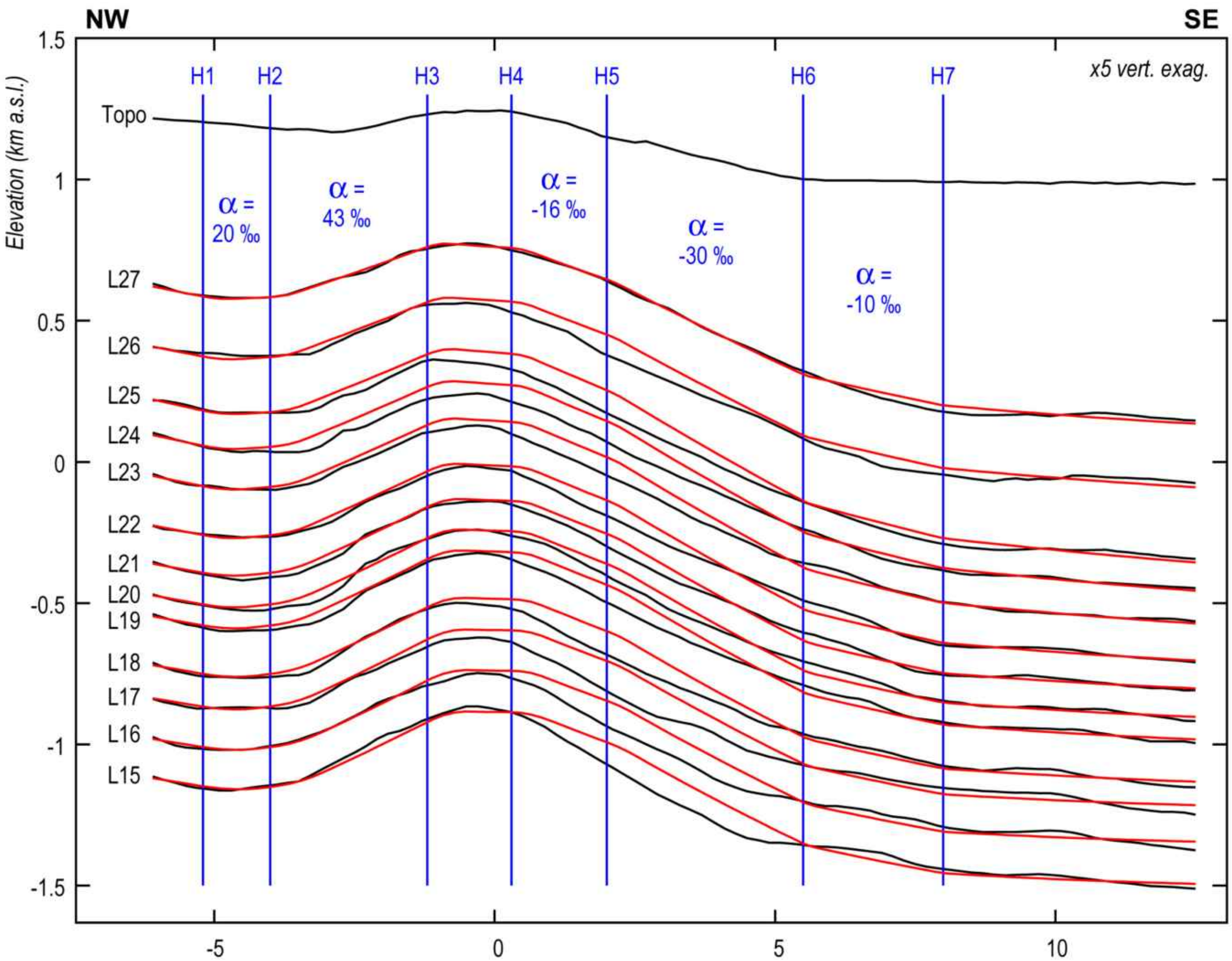

Figure 7: Parameters (in blue) of Yakeng deformation model. Black lines mark topography and observed seismic markers L15 to L27. Red lines mark the model-predicted geometry of markers, assuming the initial geometry shown in figure 5, and a constant shortening rate predicted by the linear regression of figure 6. We elected to primarily fit L27 rather than the more disturbed deeper markers (discussed in text).

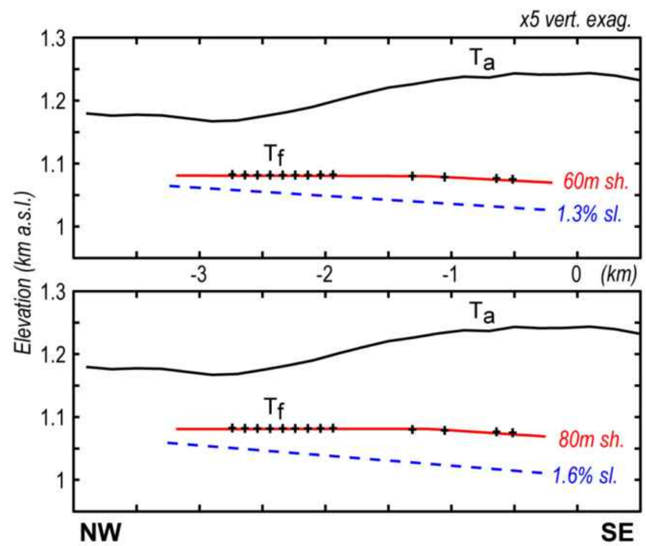

Figure 8: Models of deformed fluvial terrace Tf across Yakeng fold. Depending on the initial slope of the river terrace (1.3 to 1.6%, dashed blue, discussed in text), the amount of shortening necessary to deform it into its present-day geometry (black crosshairs) varies from 60±5 m to 80±5 m. Red lines plot the predicted Tf geometry.

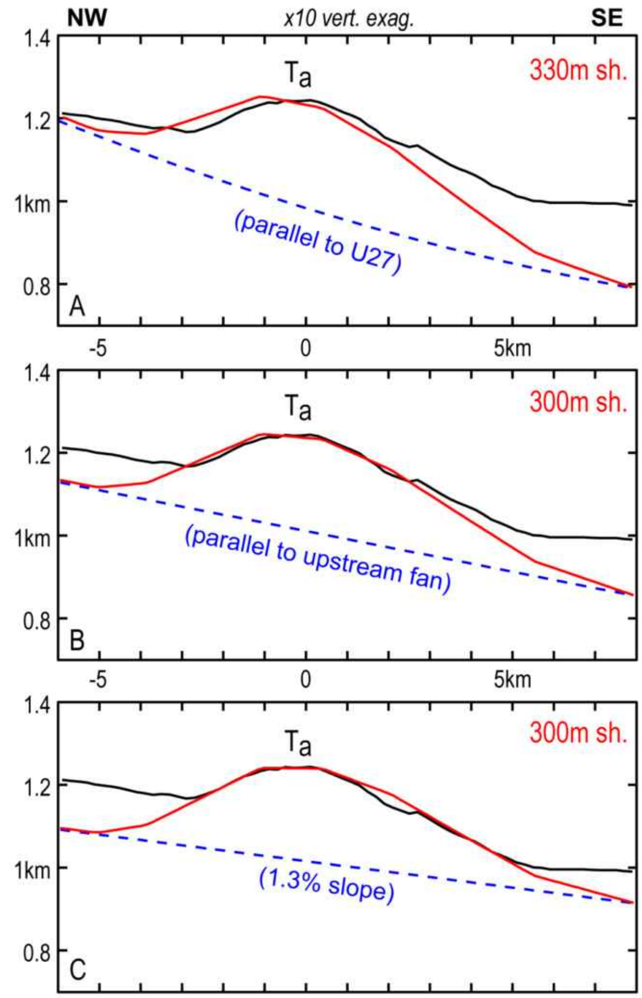

Figure 9: Models of deformed alluvial terrace Ta across Yakeng fold. Original geometries are in dashed blue, predicted ones in red and the actual topography in black. (A) Best-fitting model assuming an initial geometry of Ta parallel to that of L27. Predicted geometry differs significantly from observed shape of Ta. (B) Best-fitting model assuming that Ta was emplaced parallel to the modern East Quilitag fan. The fit is reasonably good except on the lower S flank of the fold. (C) Best-fitting model with initial slope considered as a free parameter. Slopes shallower than the modern surface of East Quilitag fan provide the best overall fit of Ta. Note that sequence of post-Ta sediments upstream of the fold is significantly thicker than downstream.

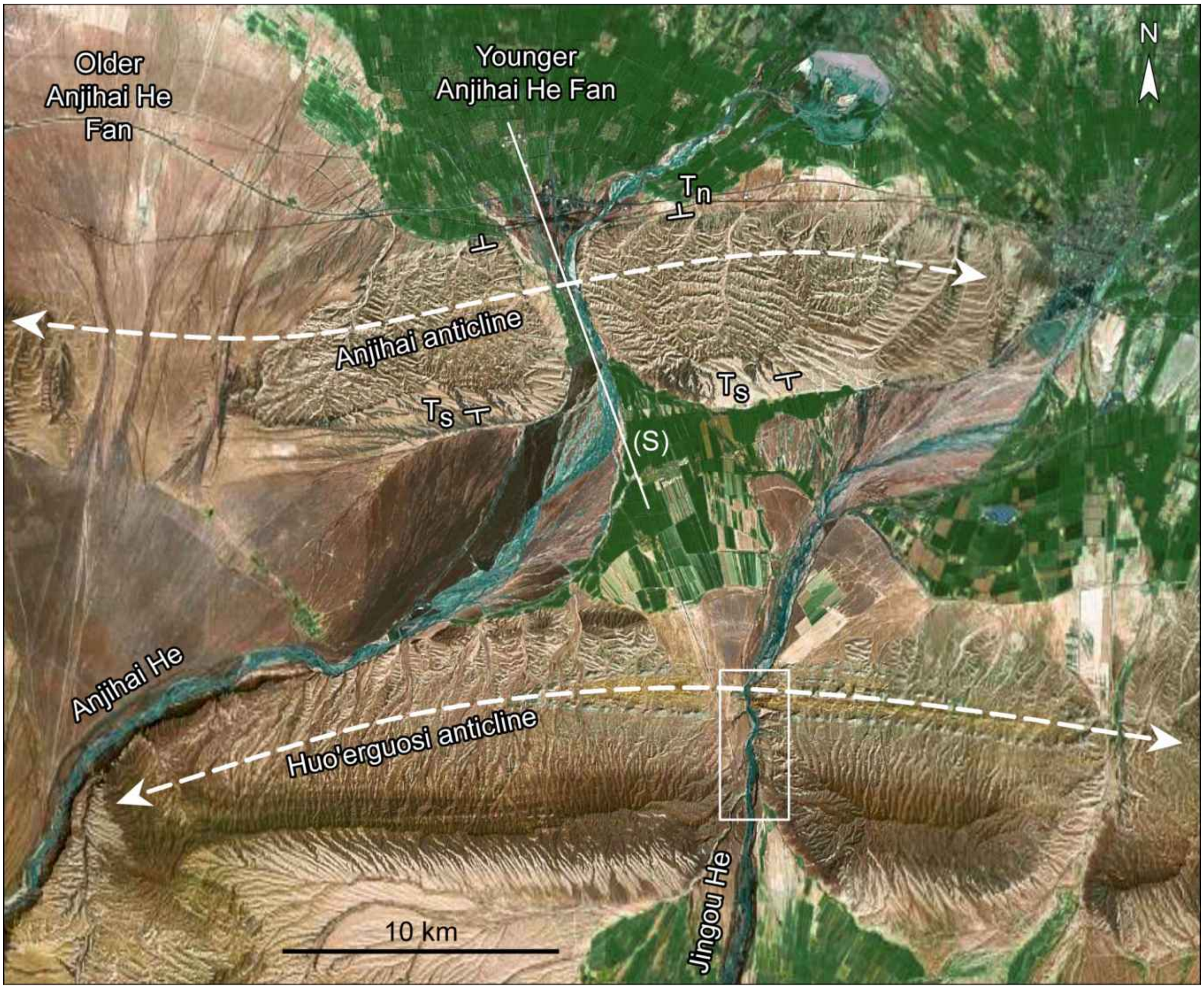

Figure 10: Map of Anjihai. Solid white line (S) marks location of seismic profile [*Dengfa et al.*, 2005]. White "T" marks indicate dips of abrasion terraces Tn and Ts. White box shows the location of magnetostratigraphic section of *Charreau* [2005] across Huo'erguosi anticline.

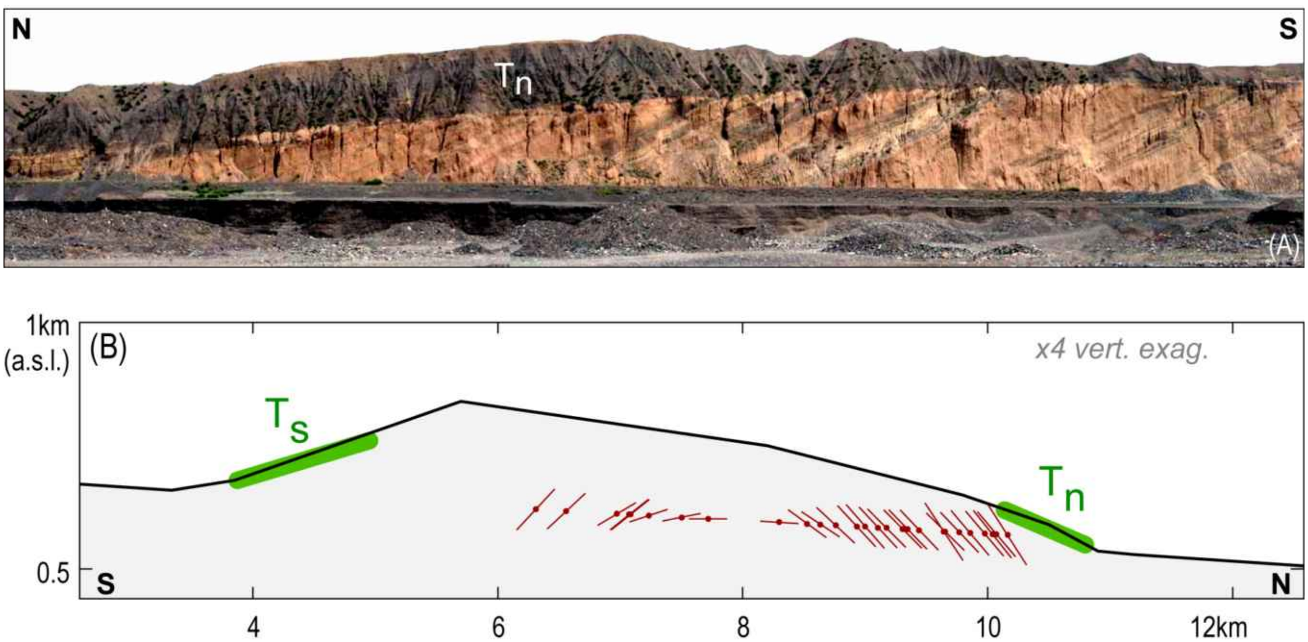

Figure 11: Geomorphic markers recording folding at Anjihai. (A) E-looking field photograph of loess-covered abrasion terrace Tn, unconformably overlying older alluvial gravel fanglomerates exposed by fluvial incision. (B) Sketch of available surface records of folding. Black line follows topographic cross-section. Green segments mark positions of well-preserved terraces Tn and Ts. Red lines plot projected dips of surface structural measurements.

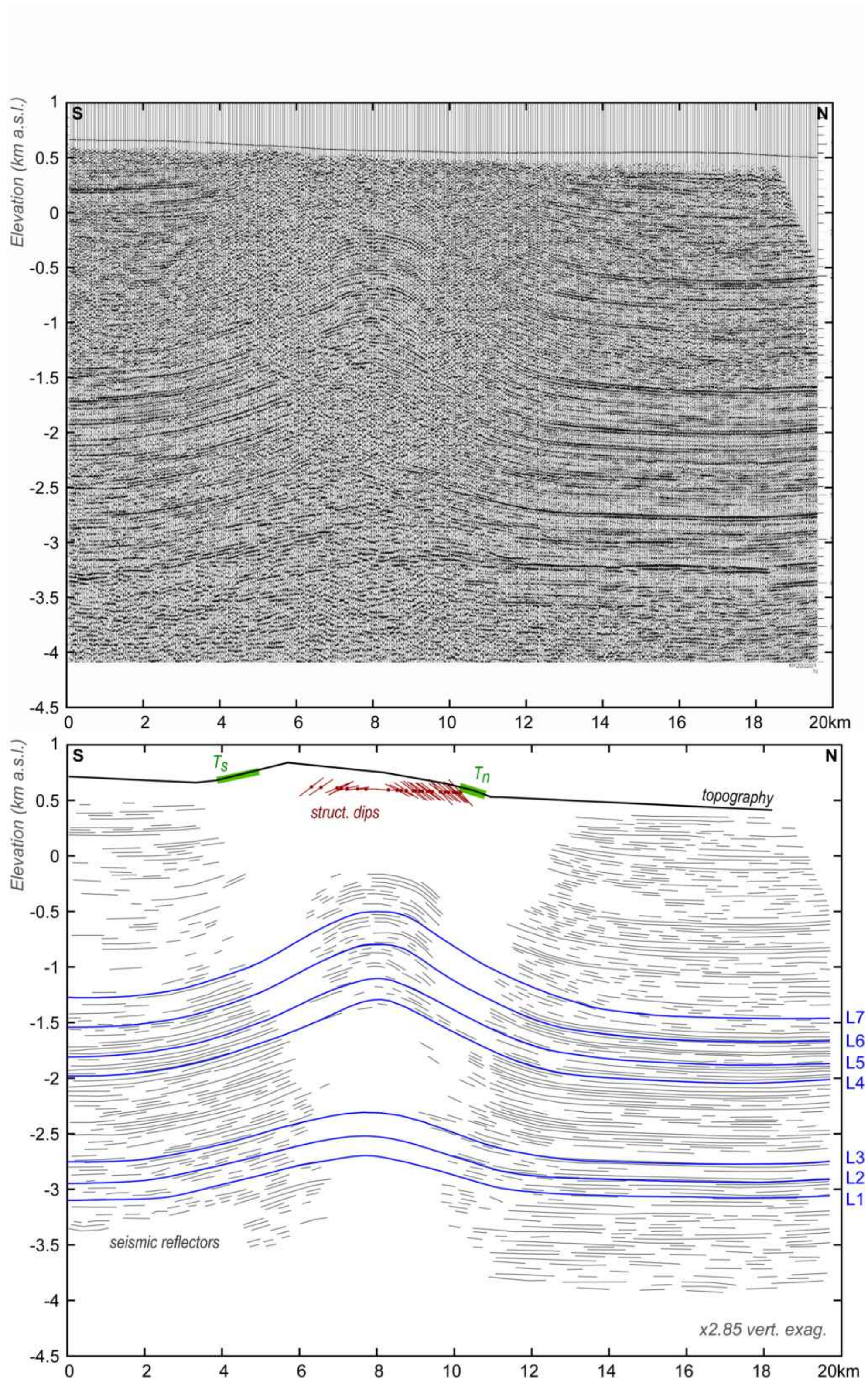

Figure 12: Seismic profile across Anjihai [*Dengfa et al.*, 2005] and our line-drawing interpretation (grey segments). Seven continuous reflectors (blue lines L1 to L7) can be mapped across the fold.

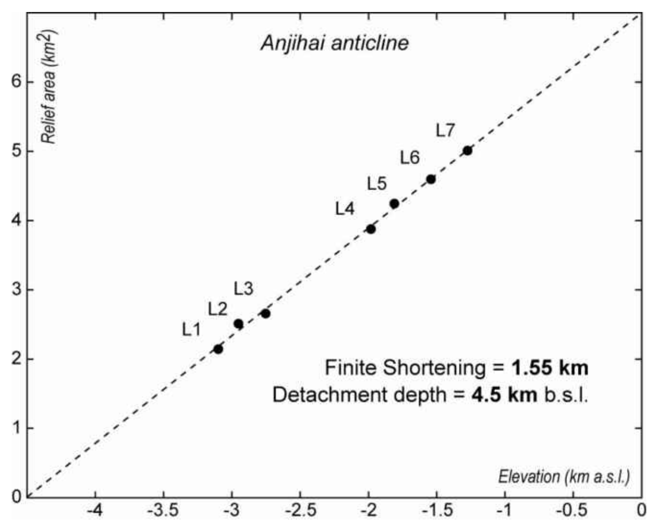

Figure 13: Plot of excess area versus stratigraphic depth for Anjihai fold. Linear fit corresponds to 1.55 km of finite shortening.

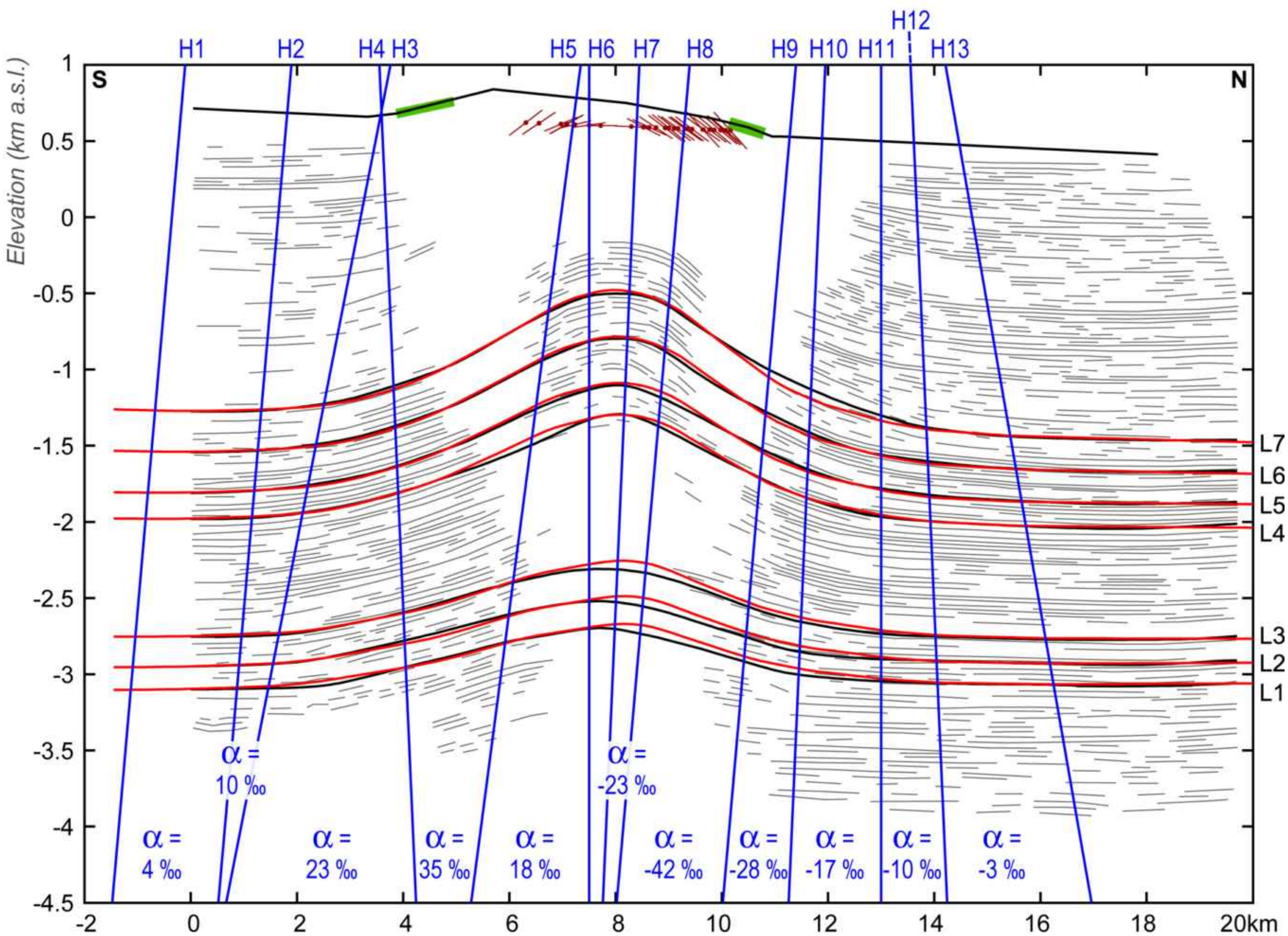

Figure 14: Parameters (in blue) of Anjihai deformation model. Black lines mark topography and observed continuous seismic reflectors L1 to L7. Red lines mark the model-predicted geometry of reflectors, using the finite shortening measured in figure 13.

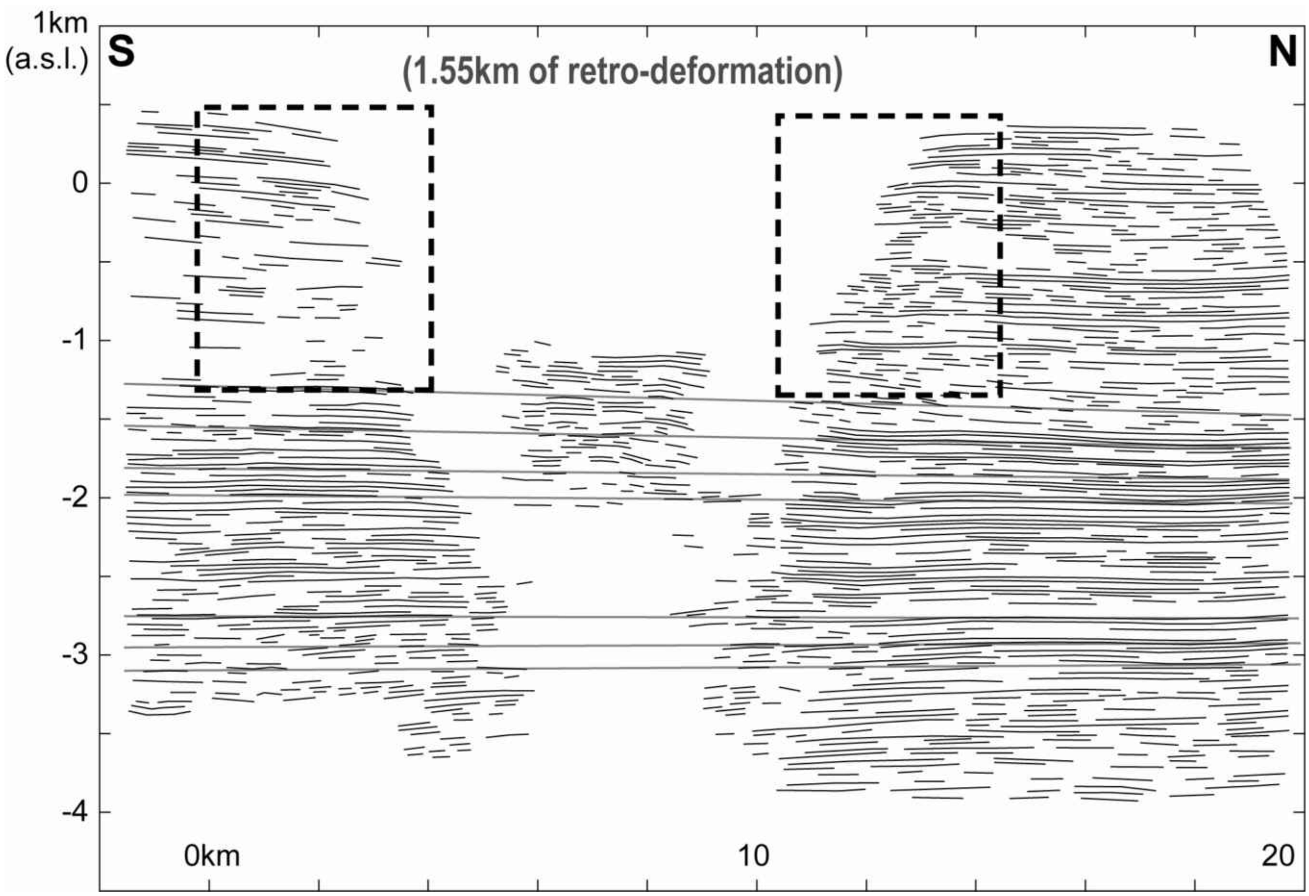

Figure 15: Anjihai seismic reflectors, retro-deformed using the parameters from figure 14 and the finite shortening deduced from figure 13. Shallow reflectors near fold core (dashed black boxes) have recorded only part of finite shortening, as evidenced by their retro-deformed dips.

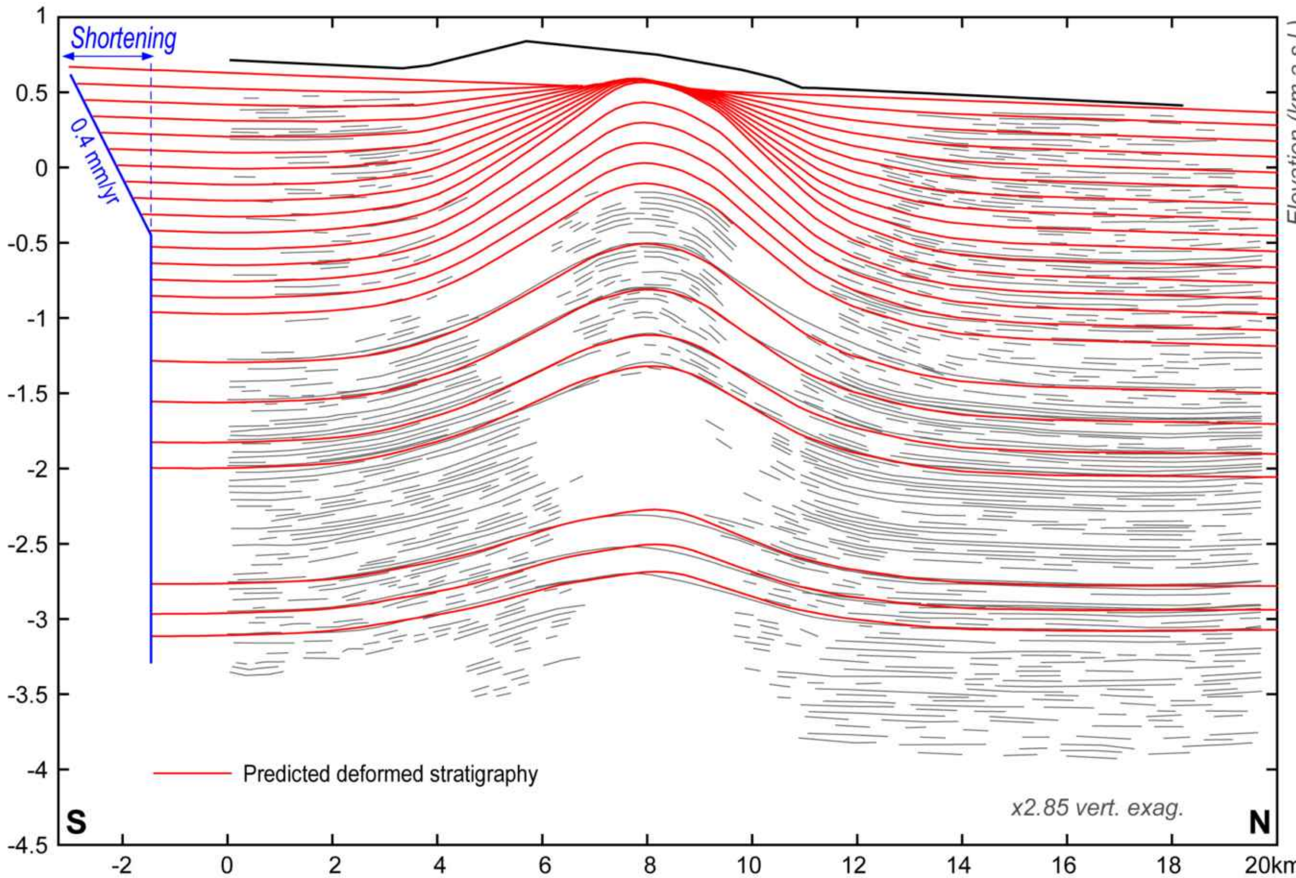

Figure 16: Predicted structure of Anjihai fold assuming a constant ratio of shortening versus sedimentation rates. This model predicts only negligible topographic relief, at odds with observed morphology.

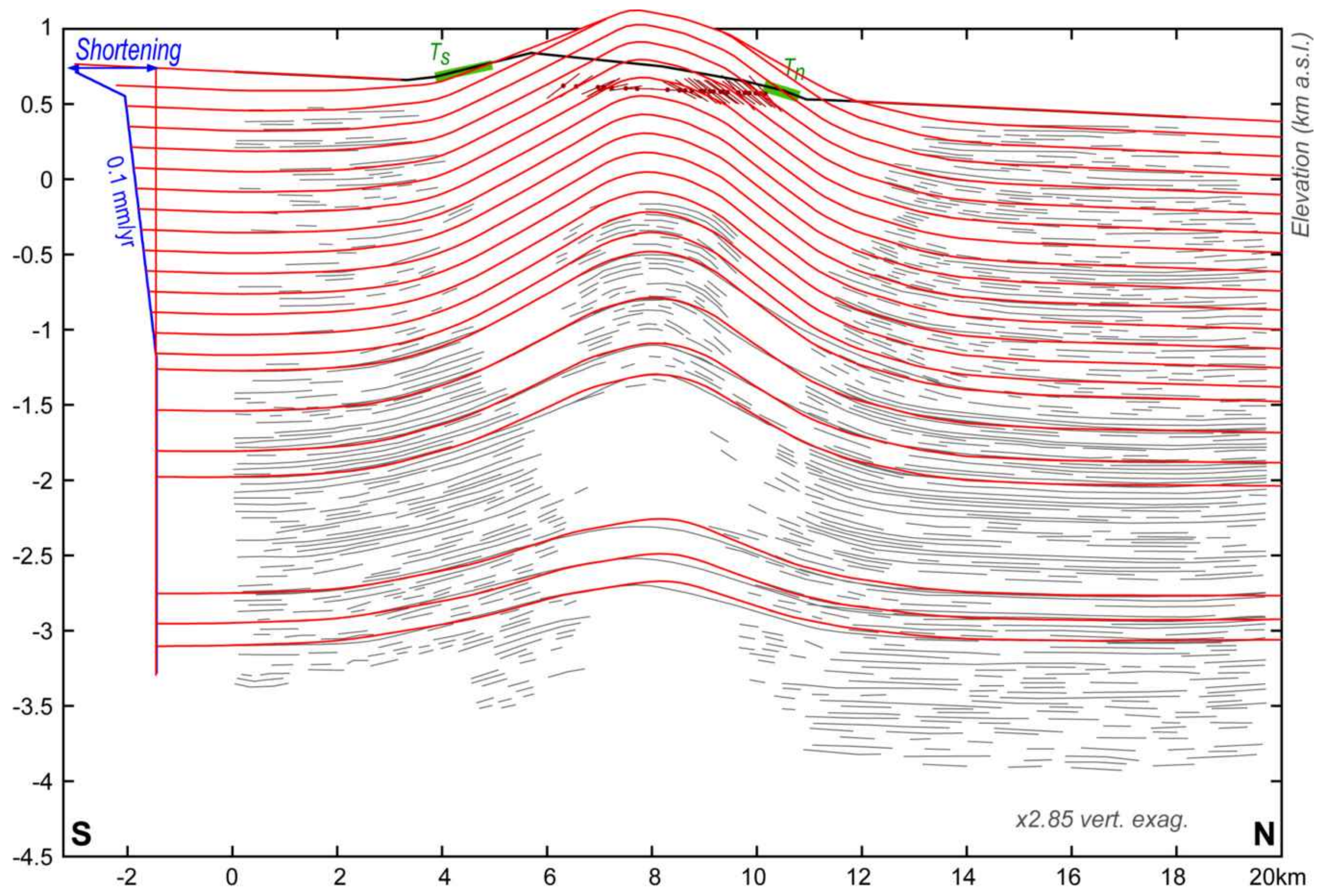

Figure 17: Predicted structure of Anjihai fold assuming a two-phase shortening history. This model fits the observed topography and structural dips, but fails to model Tn and Ts as a single, coeval surface.

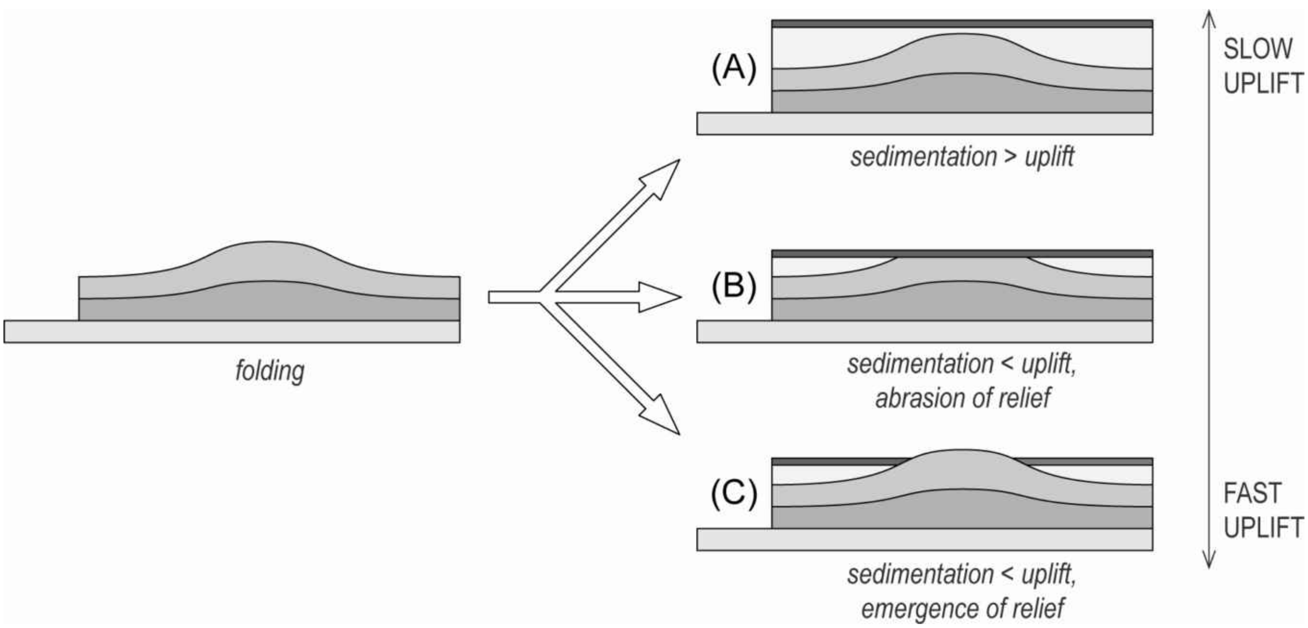

Figure 18: Summary of fold growth accounting for interactions between uplift, sedimentation and erosion (see discussion in text).

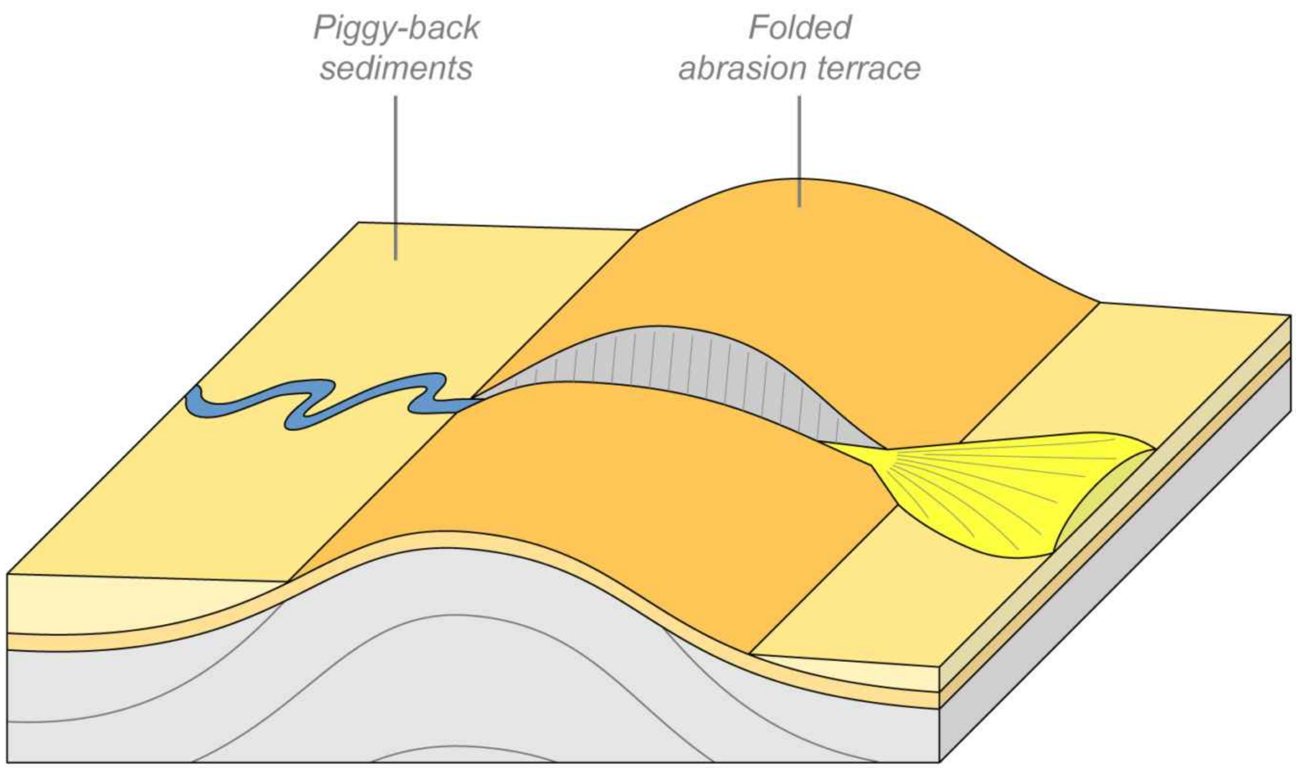

Figure 19: Surface expression of fold after relief emergence, corresponding to figure 18C. Sedimentation is perturbed by rapid accumulation of sediments upstream of fold, in piggy-back basin, and by secondary alluvial fans downstream of it.

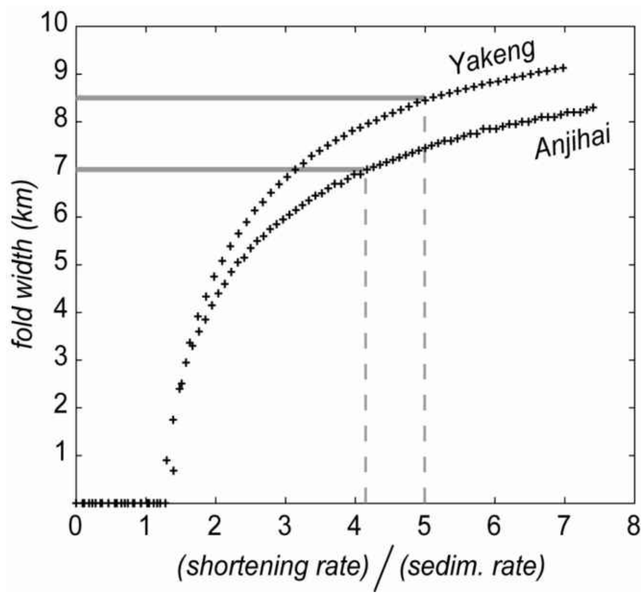

Figure 20: Predicted fold width at the initiation of relief emergence, as a function of the ratio of shortening and sedimentation rates. The observed fold widths correspond to ratios of 5.0 (Yakeng) and 4.15 (Anjihai). Combined with the relevant magnetostratigraphic sedimentation rates, these ratios imply modern shortening rates of 2.15 and 1.12 mm/yr, respectively.

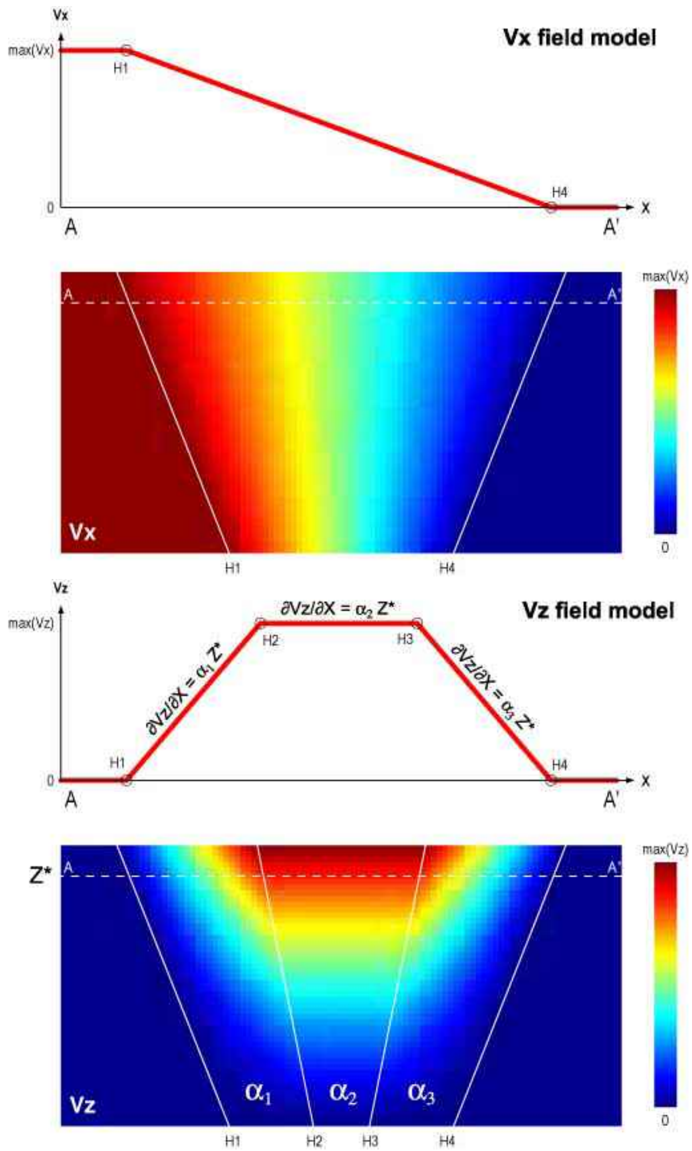

Figure A1: Simplified plot of Vx and Vz dependence on (X.Z) used in our folding models, modified from *Bernard et al.* [2006].